Arabian Journal for Science and Engineering (2023) 48:2889–2903
https://doi.org/10.1007/s13369-022-07026-7

RESEARCH ARTICLE-MECHANICAL ENGINEERING

Effects of SiC on the Microstructure, Densification, Hardness and Wear Performance of TiB_2 Ceramic Matrix Composite Consolidated Via Spark Plasma Sintering

Samson D. Oguntuyi[1,4] · Mxolisi B. Shongwe[1] · Lerato Tshabalala[2] · Oluwagbenga T. Johnson[3,4] · Nicholus Malatji[1]

Received: 4 December 2021 / Accepted: 5 June 2022 / Published online: 3 July 2022

Abstract
Monolithic TiB_2 are known to have a good combination of densification and hardness, which are sometimes helpful but limited in application. However, their usage in service at elevated temperatures such as in thermal power plants, cutting tools, tribological purposes (mechanical seals, blast nozzles, wheel dressing tools), etc. leads to catastrophic failure. Hence, the introduction of sintering additives in the TiB_2 matrix greatly influences the sinterability and properties (fracture toughness, wear resistance, etc.) of the resulting composite needed to meet the requirement for various industrial applications. In this study, the influence of SiC as sintering additives on the microstructure, densification, hardness and wear performance of TiB_2 ceramic was observed. Hence, TiB_2, TiB_2–10wt%SiC and TiB_2–20wt%SiC were sintered at 1850 °C for 10 min under 50 MPa. The impacts of SiC on the TiB_2 were observed to improve the microstructure and correspondingly improve the densification and mechanical properties, most especially with the composite with 20wt% SiC. Combined excellent densification, hardness and fracture toughness of 99.5%, 25.5 GPa, 4.5 MPa.$m^{1/2}$ were achieved, respectively, for TiB_2–20wt%SiC. Diverse in-situ phase and microstructural alterations were detected in the sintered composites. It was discovered that the in-situ phase of TiC serves as the contributing factor to the enhanced features of the composites. Moreover, the coefficient of friction and wear performance outcomes of the synthesized composites described a decreased coefficient with an enhanced wear resistance via the increasing SiC particulate. However, applying the load from 10 to 20 N increased the wear rates.

Keywords Microstructure · Densification · Hardness · Wear performance · TiB_2 · SiC

1 Introduction

Titanium diboride (TiB_2) is among the family of transition metal compounds that are regarded as ultrahigh temperature ceramics [1]. TiB_2 ceramic matrix possesses some excellent properties such as chemical stability in harsh environments, high melting points, good thermal conductivity, good abrasion resistance, high strength and hardness [2–4]. These properties have made it possible for TiB_2 to be used in various applications, viz aluminum evaporator boats, cutting tools, ballistic armour, wear-resistant parts and many more [5, 6]. Despite the excellent performance of these materials in service, their poor self-diffusion coefficient, high melting point, the existence of oxide contaminants (B_2O_3 and TiO_2) on the powder surface of TiB_2 and strong covalent bonding pose some challenges in the densification of its monolithic form [6–8]. Previous works have stated that in achieving a theoretical density of more than 98% of a monolithic TiB_2, an

✉ Samson D. Oguntuyi
samsoniumdare@gmail.com

1 Department of Chemical, Metallurgical and Materials Engineering, Tshwane University of Technology, Private Bag X680, Pretoria 0001, South Africa

2 Council for Scientific and Industrial Research (CSIR), National Laser Center, P.O Box 395, Pretoria 0001, South Africa

3 Department of Mining and Metallurgical Engineering, University of Namibia, Private Bag 13301, Ongwediva, Namibia

4 Department of Metallurgy, School of Mining, Metallurgy and Chemical Engineering, Faculty of Engineering and the Built Environment, University of Johannesburg, P.O Box 524, Johannesburg, South Africa

elevated consolidation temperature with high external pressure is required. However, grain growth developed at these high consolidation temperatures often reduces the flexural strength and fracture toughness as well as some of its intrinsic properties [9, 10]. Thus, numerous works have been done to enhance the mechanical properties and the sinterability of TiB_2 ceramics materials by introducing non-metallic additives and metallic as sintering aids. Metallic additives such as Fe, Al, Ti, Cr, Ta, etc., are applied for TiB_2 ceramic densification. However, their usage is limited due to their depreciating effects on the high-temperature application of TiB_2. Owing to these challenges, attention has been shifted to densifying TiB_2 using non-metallic additives which are mostly carbides, silicides, nitrides and boride-based sintering aid such as AlN, TiC, WC, Si_3N_4, NbC, SiC and ZrB_2 [11–14]. These additives remove oxide layers from the powder surface or create in-situ phases that contribute to the composites' sinterability and enhancement of properties [12, 15, 16].

Spark plasma sintering (SPS) is one of the novel fabrication processes used to consolidate TiB_2 ceramic materials. Because this technique uses a lower temperature to achieve the densification of ceramic materials under low pressure at a short dwell time. These features have made SPS gain high predominance over other conventional sintering, specifically hot press, hot isostatic press, etc. The application of SPS ensures the achievement of high densification, finer microstructure and excellent mechanical properties [17–19].

In addition, the importance of fine microstructure, peak densification and excellent mechanical properties cannot be jettisoned in the enhancement of wear performance. Hence in achieving these features, judicious selection of the type of sintering additives/matrix and their right composition has a lot of priority. The utilization of ceramic matrix composites for cutting tools and other applications where wear behavior is highly considered, certain things must be measured to design the type of materials that can withstand the wear rate. Thus, the type of load, time and the type of medium the material will be used will be put into consideration. It has been studied that under dry sliding parameters that the tribological performance of ceramic components is complicated and reliant on some external conditions such as sliding speed, humidity, temperature, load counterpart atmosphere, etc. [20, 21].

Past works have emphasized the influence of carbides and nitrides reinforcement on borides ceramic's relative density and mechanical features. The inclusion of 5 wt% silicon nitride (Si_3N_4) in TiB_2 ceramic matrix as a sintering aid was observed. It was reported that there was a densification increment when it was sintered via SPS at the temperature of 1900 °C under 40 MPa for 7 min. [4]. It was reported that the incorporation of 2.5 wt% Si_3N_4 to TiB_2 matrix enhances the sinterability of the composites significantly when it was hot-pressed at 1800 °C for 1 h [6]. The examination of the impact of diverse composition of SiC particulates under varying sintering parameters (at 1600–1800 °C, under 10–30 MPa for 5–15 min) was studied on the consolidation of TiB_2 based composites. A densification of 99.5% was attained at the temperature of 1800 °C under 30 MPa for 15 min. [7]. At the grain interface of the reinforcement (SiC) and the matrix (TiB_2), the secondary interfacial phase (TiC), which was created via the reaction between the surface oxide contaminants and the SiC particles, was reported to improve the densification [11, 22, 23]. An examination was carried out on the influence of TiN and SiC as an additive and reinforcement on TiB_2-based composites synthesized via SPS at 1900 °C for 7 min under 40 MPa. A densification of 99.9% was achieved for the composites of TiB_2–SiC (20 vol%)–TiN (5 wt%) and TiB_2–SiC (20 vol%) [24] in contrast to the undoped TiB_2 with densification equal to 96.7% under a similar sintering parameter [4]. The inclusion of TiN and SiC was reported to form in-situ phases, which concurrently improve the densification and sinterability of the two samples [4, 25, 26]. The finer microstructure was examined to be produced because of the addition of TiN. This experimental work also concurs with Shayesteh et al. [27], when he only used TiN as a dopant for TiB_2. Alexander et al. [28] studied the wear performance of B_4C-carbon nanotube. They achieved a specific wear rate of 1.06×10^{-6} mm^3/N.m, which was less than the undoped B_4C ceramics, hence depicting the impact of carbon nanotube in the improvement of B_4C composites wear performance. Murthy et al. [29] examined that the addition of ZrO_2 to B_4C ceramic matrix was observed that an in-situ ZrB_2 and similarly round pores of sub-micron size were formed. Also, the establishment of CO gas was detected to aid in the arrest or deflect cracks, thus enhancing the tribological behavior of B_4C ceramics. Sharma et al. [30] stated that with a rise in load, the specific wear rate of SiC composite declines and then the coefficient of friction initially increases and then declines when there is an increase in the sintering additives of WC from 0 to 50 wt%. Sonber et al. [31] studied the tribology behavior of B_4C when WC ball was used as the cemented counter body. They discovered that the specific wear rate of B_4C increases with a rise in load and consequently, its coefficient of friction declined.

Profound works have been carried out on the microstructure, densification and mechanical properties of TiB_2 using SiC as a sintering additive. However, little or no work has been reported on the influence of microstructures and mechanical properties of this composite on its wear performance. Therefore, in this study, the impacts of SiC on the microstructure, relative density, mechanical properties and the wear performance of TiB_2 ceramic were observed, and more importantly, the influence of these aforementioned properties on the wear behavior of TiB_2–SiC was studied.

2 Experimental Procedure

2.1 Materials and Process

(a) Powders and Sample Preparation

The starting available powder TiB_2 (purity: 99.5%) produced by H.C. Starck Berlin Werk Goslar, SiC powder (purity: 99.5%), produced by USA (F.J. Brodmann & Co.) were applied as it is stated in Table 1. The initial powder, such as Titanium diboride, was used as a matrix, silicon carbide was used as a reinforcement in the matrix ceramics. The powders were prepared into two varying compositions of powder viz, TiB_2–10wt%SiC and TiB_2–20wt%SiC. The XRD of the as-received powders and the mixed compositions are shown in Figs. 2 and 4. The compositions were mixed in a tubular mixer ((WAB TURBULA SYSTEM SCHATZ)) at a revolution of 78 rpm for 6 h.

TiB_2–10wt%SiC and TiB_2–20wt%SiC were discharged in a graphite die (having an inner diameter of 20 mm). The graphite foil is placed between the powder and the die walls and between the punch and the powder. The graphite foil was used to prevent friction between the die and the powder during the consolidation process and also for easy removal of the as-sintered compact after the consolidation process. The sinter chamber during the experiments was kept under a vacuum of 10^{-2} torr, which is equivalent to 1.3332 Pa. It is worth mentioning that the reason why this pressure value was chosen is to eliminate any air in the chamber which could interfere with the consolidation process of the samples at high temperatures. Then via the pyrometer attached to the grafoil die, the sintering temperature was observed, controlled and measured. The heating rate of 150 °C/min was induced by an alternating current along with a frequency of 50 Hz. This was done until the sintering temperature was raised to the specified temperature (1850 °C). A pressure and dwell time of 50 MPa and 10 min were employed during the sintering cycle. Before removing the sintered compacts from the sintering chamber, they were allowed to cool at normal temperature. The cooled samples were sandblasted to eliminate any contaminants of the graphite (placed between the surface of the powder and the die) on the surface of the sintered samples.

(b) Characterization of the Sintered Samples

The relative density of the as-sintered compacts was calculated via a densitometer which is established on Archimedes principle. For the metallographic analysis, metallographic techniques were used to prepare the transverse cuts of the sintered samples. The compacted sintered samples were ground by abrasives emery papers of different grit sizes 320, 400, 600, 800, 1200, 1400 and polished with diamond suspensions (sizes 1, 3 and 6 μm), with Kroll's reagent (2 ml HF, 92 ml H_2O and 6 ml HNO_3). The elemental, topography and microstructure of the sintered compacts were observed and analyzed via 7600F field-emission scanning electron microscope (FESEM, JEOL 7600F) with energy-dispersive X-ray spectroscopy (EDS). The X-ray diffractometer (XRD, PW1710 Philips) was used for phase identification.

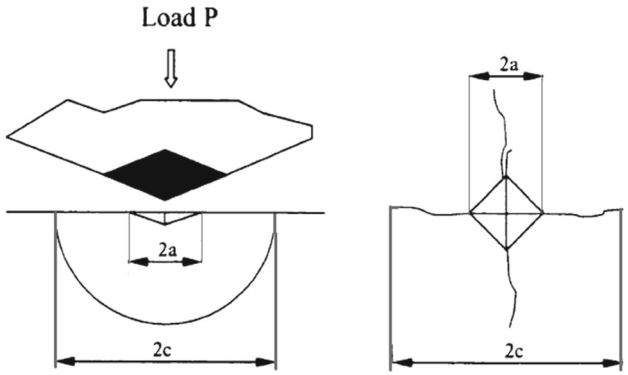

Fig. 1 Representation for Vickers hardness and indentation test for fracture toughness

The micro-hardness tester (FM-700 FUTURE-TECH) was used to determine the Vickers microhardness. A force of 2 kg with a dwell time of 15 s. For each sample, 10 measurements were carried out, and the mean value of the results was obtained in (GPa) value for the sintered sample. The fracture toughness was estimated via the crack length measurement created by the indenter as revealed in Fig. 1. At a load of 2 kg, the measurement (crack length) was done with an optical microscope. Then the formula suggested by Fukuhara et al. [32–34] Eq. 1 was used to estimate the fracture toughness of the sample

$$K_{ic} = 0.203\mathrm{Hv}\, a^{1/2}(c/a)^{-3/2} \quad (1)$$

where Hv—Vickers hardness, 2*a*—diagonal of the indenter, 2*c*—total indentation crack length.

At least five indentation examination and their mean value of the data were reported.

(c) The Examination of Dry Sliding Wear

The tribology test was done with (MFT-5000), RTec universal tribometer besides reciprocating wear drive to contrast diverse loads because loads govern a fundamental role in wear features of components. An exact linear platform was engaged to grip the sample attached to a rod designed to put it in motion. The motion was engaged via the exterior motor that was attached to the functioning stage. Different loads of 5 N, 10 N, 15 N and 20 N using stainless steel balls of diameter 6 mm were engaged at a linear speed of 0.06 cm/s for 900 s. The wear test was done on a square sample of size (10 × 10 mm) after its surfaces had been grounded and polished so that SEM could be used to characterize and capture the wear tracks, and thus, the worn-out surfaces can be seen clearly.

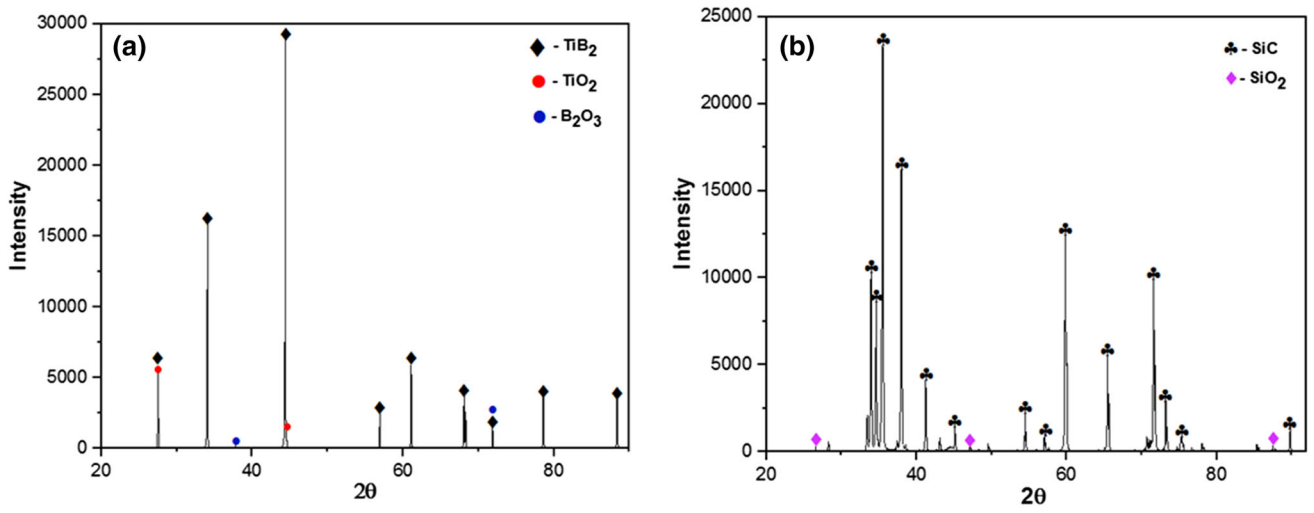

Fig. 2 XRD of the as-received powder of **a** TiB_2, **b** SiC

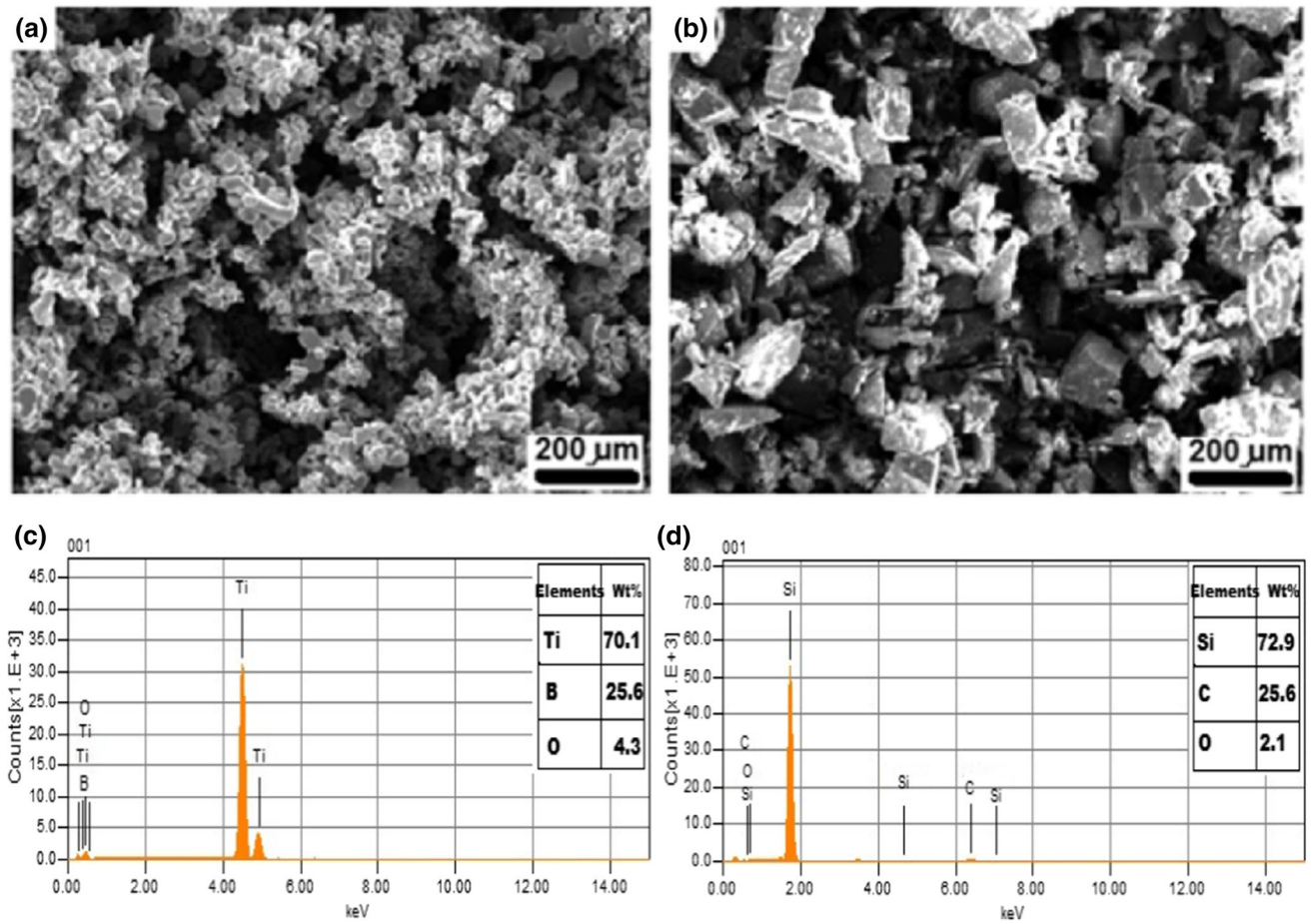

Fig. 3 SEM images and EDX of the as-received powder of TiB_2 (**a**, **b**) and SiC (**c**, **d**)

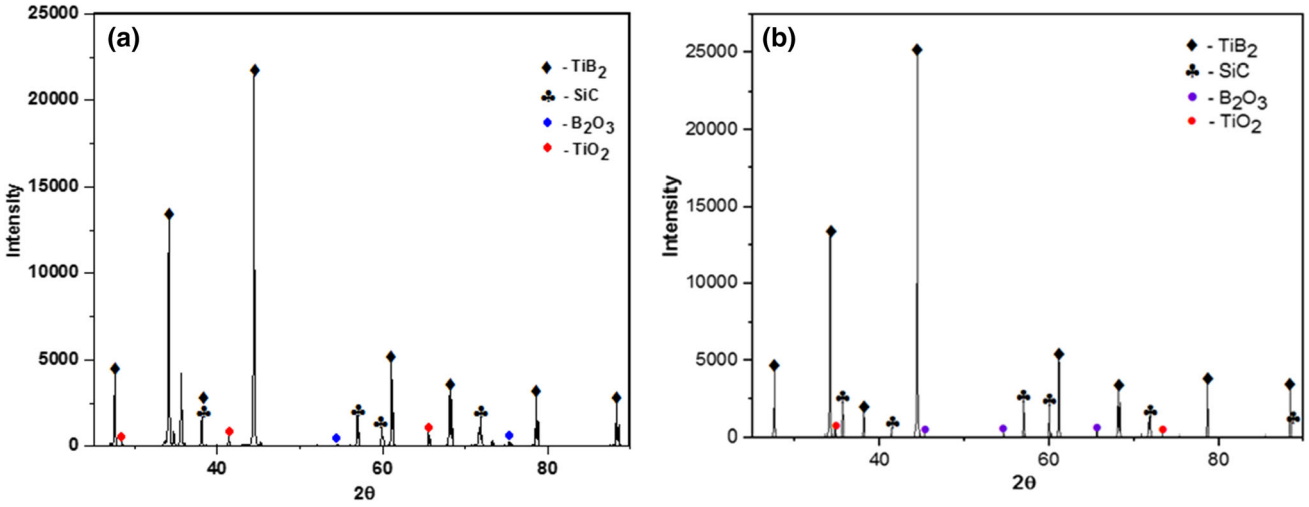

Fig. 4 XRD of mixed composites **a** TiB_2–10SiC, **b** TiB_2–20SiC

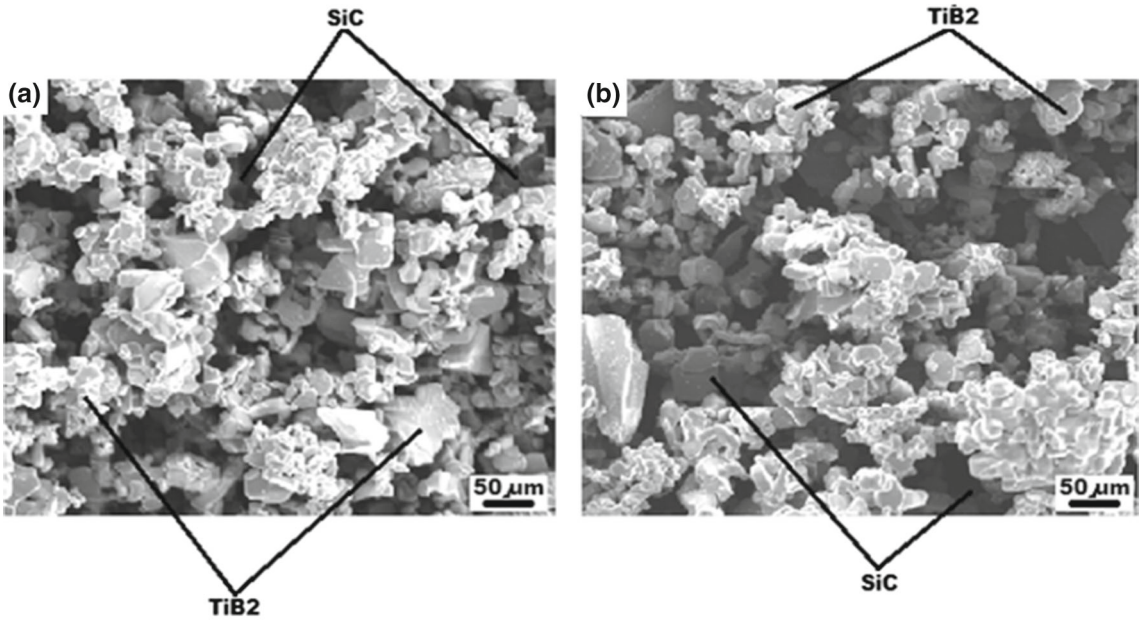

Fig. 5 SEM micrograph of admixed powder **a** TiB_2–10SiC, **b** TiB_2–20SiC

3 Results and Discussion

3.1 The Characterization of Feedstock Powder and Mixed Powder

The features of the as-received TiB_2 matrix and sintering additive of SiC are shown in Figs. 2 and 3, and their elemental compositions are shown and analyzed via EDX (Fig. 3). Furthermore, the XRD observation detected that the peaks are mainly of TiB_2 and SiC. However, there are discoveries of some oxide contaminants as revealed by the XRD and EDX analysis. B_2O_3 and TiO_2 are seen on the TiB_2 surface, while SiO_2 is detected on the SiC surface. These types of contaminants can be associated with the covering oxide layers which are created on the surface of non-oxide ceramics. The mixed composites (TiB_2-10SiC and TiB_2-20SiC) examined via the XRD (Fig. 4) and SEM (Fig. 5) depicted that there is an obtainment of uniform distribution of the powder matrix and the reinforcement.

3.2 Relative Density

Figure 6 reveals the densification of the as-sintered composites. It was observed that there was an increase in densification as the SiC increased from 10 to 20% in the composites. The percentage increment of the composite

Table 1 The description of the as-received powder

Materials	Particle shape	Density	Particle size	Purity (%)	Supplier
TiB_2	Irregular	4.52	5.1 micron	99.5	H.C. Starck Berlin Werk Goslar
SiC	Irregular	3.21	− 325 Mesh	99.5	USA (F.J. Brodmann & Co.)

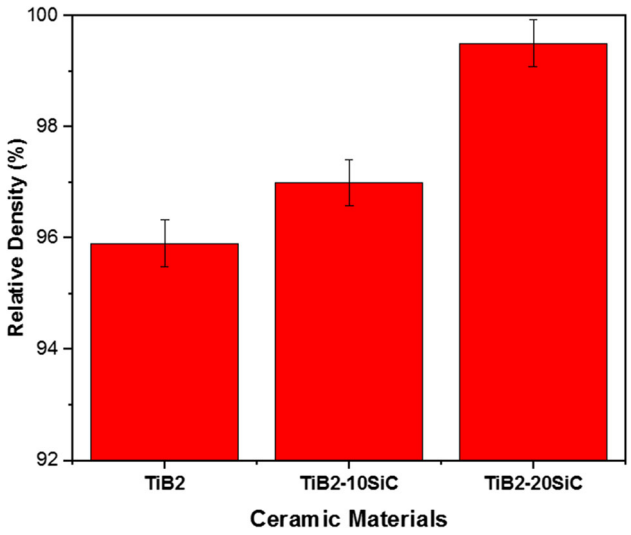

Fig. 6 Relative density of monolithic TiB_2 and doped TiB_2–SiC

TiB_2–10 SiC and TiB_2–20 SiC in contrast to the undoped TiB_2 are 1.12% and 3.6%, respectively. The development performance of the doped sample is being credited to the emergence of in-situ phases such as TiC, whose properties will be later discussed. Figure 6 gives the correlation between the undoped TiB_2 and the doped TiB_2 with SiC. The graph depicts that with increasing SiC composition, the composite of TiB_2–10 SiC and TiB_2–20 SiC have their relative density equivalent to 96.99% and 99.50%, respectively, in contrast to the undoped TiB_2 with densification equal to 95.9%. This outcome infers that the fraction percentage of SiC improves the relative density and sinterability of TiB_2. In addition, the sintering parameter of 1850 °C/50 MPa/10 min was observed to be of great influence for the composites, as it minimizes the establishment of pores on the surface of the sintered composites.

3.3 Microstructural Evaluation of Sintered sample

Figure 9b, c depicts that the grains of the as-sintered composites are wholly connected, signifying an excellent sinterability between the matrix and the reinforcement. Hence, the existence of several in-situ interfacial phases is more significant in the sample with a higher percentage of reinforcement (TiB_2–20SiC) than the sample with less reinforcement (TiB_2–10SiC). No notable grain growth was detected during the SPS. The introduction of SiC was observed to inhibit grain growth in TiB_2-based ceramics. Thus, the attained fine-grained microstructure of the doped TiB_2 was not only credited to the existence of SiC and some various formed in-situ secondary phases especially TiC but also to the relatively short dwell time and the lower sintering temperature of the SPS which also contributed to the reduced grain growth. The practical impact of SiC has similarly been examined in the consolidation of ZrB_2-based composites. The introduced SiC with the use of lower sintering temperature was detected to minimize grain growth [35–37]. XRD spectra depicted in Fig. 7 confirmed the presence of secondary or in-situ phases in TiB_2–10SiC and TiB_2–20SiC composites. A synonymous work carried out by Ahmadi et al. [25] stated that on the surface of the starting powder of TiB_2, there was a development of B_2O_3 and TiO_2 oxide layer. Although the oxygen content was observed to decline, this was due to the sintering manner caused by the chemical reactions. The achievement of the reaction between the oxide layer of SiC and TiO_2 produced some products of SiO_2 and TiC, and this was examined by HSC chemical software (Eq. 2). The Gibb's free energy for this reaction is − 80 kJ, signifying a thermodynamic approval. The creation of in-situ phases of TiC and SiO_2 vindicated the validity of the reaction as depicted via the XRD patterns (Fig. 7).

$$TiO_2 + SiC - TiC + SiO_2 \quad (2)$$

Moreover, the development of SiO_2 attained during the consolidation procedure can promote the relative density enhancement in the sintered compact composite via the liquid phase sintering mechanism. The sintering temperatures for melting and boiling of the B_2O_3 oxide layer are at 450 °C and 1860 °C in the atmospheric condition of 1 atm, respectively. The evaporation of B_2O_3 occurs at a temperature less than 1600 °C, and this achievement is credited to the stages of the sintering atmosphere vacuum. Finally, the oxide layer of B_2O_3 combines with SiC, as established in Eq. 3, generating B_4C and various byproducts in the gaseous phase. Thermodynamically, Eq. 3 is attainable at temperatures of 1750 °C or above [38].

$$4B_2O_3 + 7SiC - 2B_4C + 7SiO + 5CO \quad (3)$$

For clarity purposes, the elemental composition of the sintered composite (TiB_2-20SiC) is analyzed in the EDX

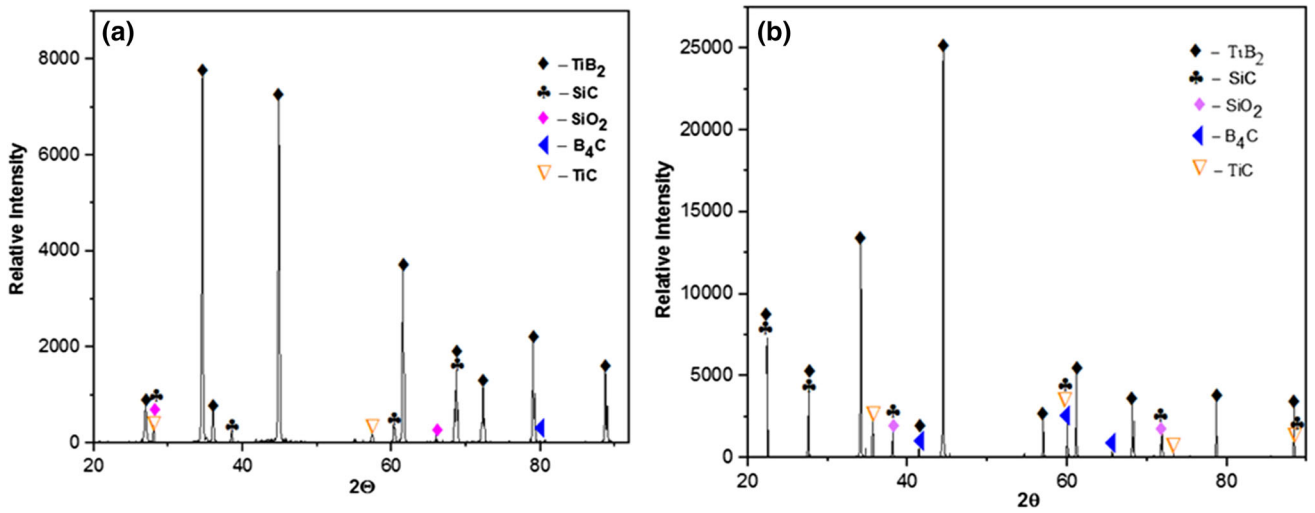

Fig. 7 XRD of as-sintered **a** TiB_2–10SiC, **b** TiB_2–20SiC

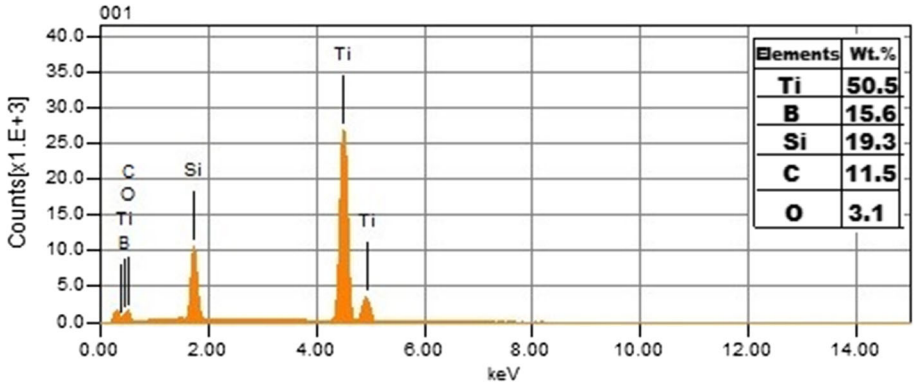

Fig. 8 EDX of sintered TiB_2–20SiC

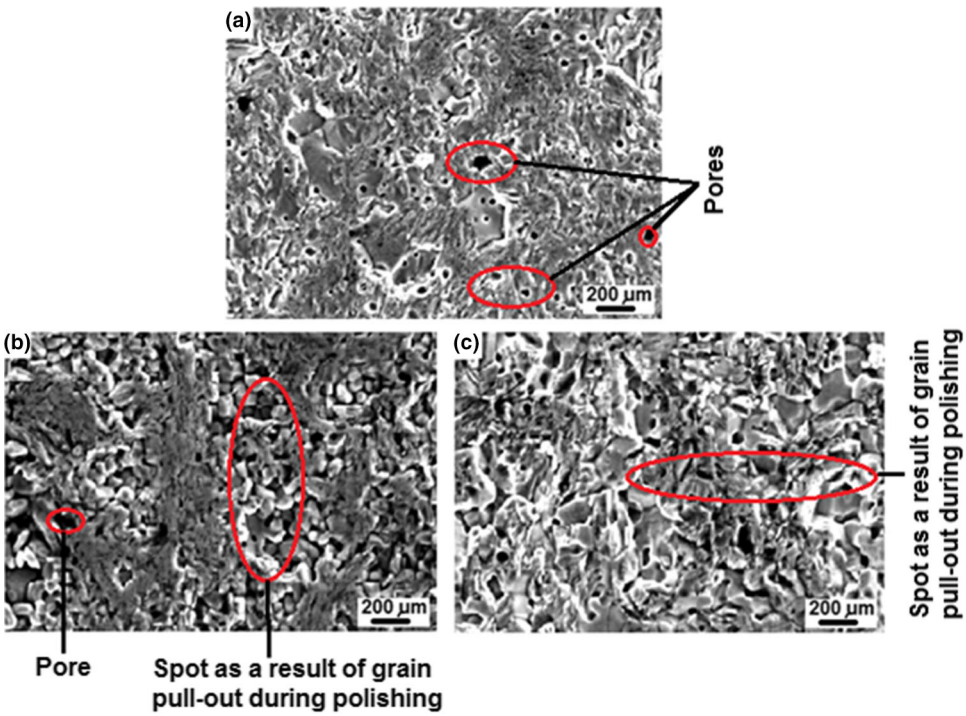

Fig. 9 SEM images of polished sintered **a** monolithic TiB_2, **b** TiB_2–10SiC and **c** TiB_2–20SiC

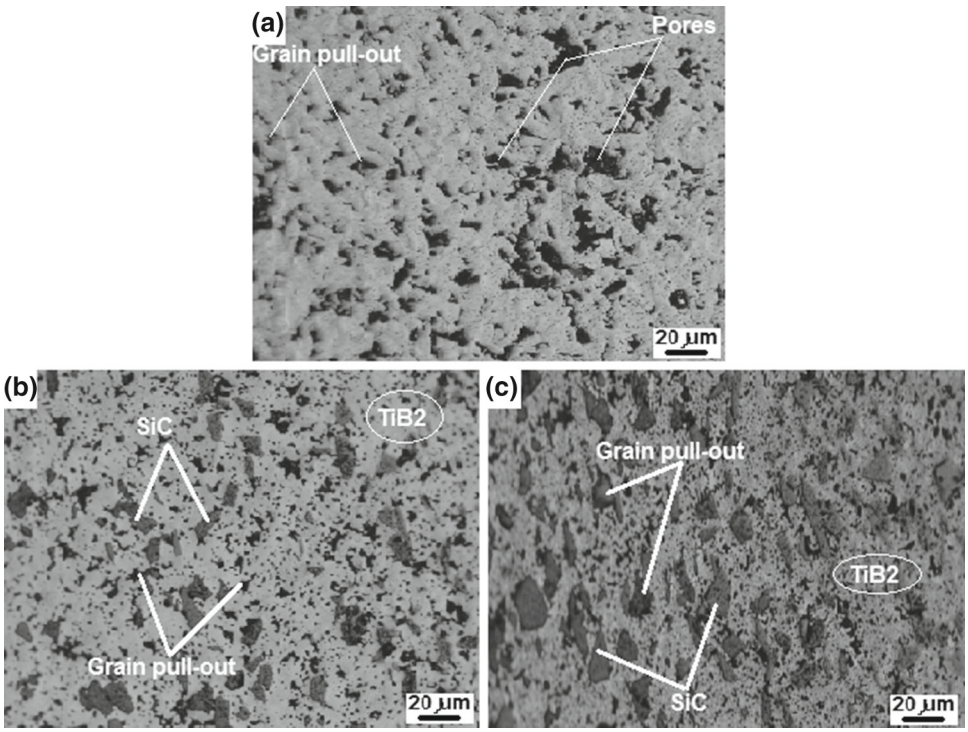

Fig. 10 OPM of polished sintered **a** monolithic TiB_2, **b** TiB_2–10SiC and **c** TiB_2–20SiC. The grey phase is the reinforcement of SiC grains. The bright phase is the ceramic matrix grains of TiB_2 and lastly, the black phases are pores or some of the pull-out grains during polishing

(Fig. 8). Based on this EDX outcome, the grey and bright phases were identified as SiC additive/reinforcement and ceramic matrix, respectively. The black phases are either pores or the grain pull-out during polishing. Similar observations were obtained when the samples were characterized using an optical microscope (OPM), as shown in Fig. 10. A synonymous work carried out by Ghafuri et al. [39] detected a similar situation. The presence of pores in ceramic materials can reduce their density. Therefore, the measured relative density is consistent with the fractured surface images (Fig. 11), and this backed the outcomes that the porosity of TiB_2–20SiC < TiB_2–10SiC < TiB_2. The attainment of lower relative density in TiB_2 in contrast to the higher densification of TiB_2–10SiC and TiB_2-20SiC was ascribed to the surface pits and pores (Fig. 9). It has been stated that the existence of oxide contaminants on the diborides surface (e.g., HfB_2, TiB_2 and ZrB_2) not only initiates grain growth but also lowers the densification process. Thus, the introduction of the sintering additive (SiC) was observed to be beneficial in eliminating the oxide contaminants from the surface of the sintered TiB_2 and hence promoting some in-situ phases that contributed to the enhancement of the composites densification [22, 40] (Figs. 10, 11, 12).

3.4 Mechanical Properties

Regarding the experimental outcomes, it is revealed that the hardness of the sintered composites got to its peak when the 20% reinforcement (SiC) was introduced into the matrix. Hence, TiB_2–20SiC has a hardness of 25.5 GPa, which is 29.01% greater than the monolithic TiB_2 (18.1 GPa). Then the composite having 10% reinforcement of SiC (TiB_2–10SiC) has a hardness of 19.05 GPa, which is a 5% increment compared to monolithic TiB_2 (Fig. 13). For the fracture toughness, there was a huge improvement in the fracture toughness of the reinforced composites (TiB_2–SiC) in comparison with TiB_2, which was credited to the second phase of SiC. The lower outcome of the monolithic TiB_2 sample (3.30 $MPa.m^{1/2}$), as shown in Fig. 13, was majorly due to its lower densification (95.9%), and this fracture toughness improved to 3.8–4.5 $MPa.m^{1/2}$ with an increasing additive of SiC.

Microstructural features viz, second phases, porosity and grain size have huge impacts on mechanical properties. Furthermore, the hardness and fracture toughness of ceramics are affected mostly by their relative density [41]. This observation was demonstrated by the experiment carried out by Ghafuri et al. [39]. They reported that the enhanced fracture toughness and micro-hardness are credited to the reduced porosity and increased densification [3, 42]. Usually, the fracture toughness of ceramics is not only subjected to its relative density but also its grain size. The larger grain particles tend to lower their fracture toughness, which inhibits the improvement in the overall mechanical properties. Although a reduced grain size promotes more cracks deflections and grain boundaries, all these cause crack propagation allowing fracture energy consumption. Therefore, reducing grain size increases the fracture toughness of composites [43]. Balak

et al. [44] recommended that a dwell time of 8 min and a peak temperature of 1700 °C can be used to achieve the sintering of ZrB_2–SiC-based composites with enhanced properties. They further stated that the composites' fracture toughness would depreciate if the sintering conditions were increased. They upheld that increased grains would be connected with low strength to restrict crack propagation. Though higher dwell times and temperatures tend to induce open pores, and these consequently cause a reduction in fracture toughness due to grain coarsening. Hence, fracture toughness improvement is majorly controlled by grain size rather than open porosity. Crack deflection around the boundaries of the TiB_2/SiC and the SiC particles influenced a significant role in the toughening mechanism of the sintered materials. The thermal residual stress, which is initiated by the lack of congruence between the coefficient of heat expansion of the SiC grains and TiB_2, was observed to promote the crack-microstructure connections (crack deflections) [41]. The compressive stresses in the particulates phase of SiC caused a crack deflection (Fig. 12) which promotes a huge stress relaxation at the crack tip to decline the dynamic force for crack movement. Hence, the toughness of the samples is enhanced.

In addition to the fracture toughness, crack bridging and crack branching (as depicted in Fig. 12) were also recognized as the other mechanisms that contributed to the toughening effects of the composites (especially for TiB_2–20SiC). In the meantime, microcracking, similarly stated by King et al. [41], is an alternative toughening effect in the composites of TiB_2–SiC. Extra fracture energy is used up in this mechanism via microcracking due to the interfacial stress made at the SiC/TiB_2 grain boundaries. This mechanism is initiated by the lack of congruence between the heat expansion coefficient of the SiC grains and TiB_2. Therefore, a shield is created by microcracking at the tip of a propagating crack, which consequently improves toughness [45]. In summary, the fracture mode alteration from intergranular to mainly transgranular approach is initiated by introducing SiC as revealed from the fractured surface (Fig. 11), hence the crack movement energy is caused by combining the toughening mechanism during the fracturing process which improves the fracture toughness.

3.5 The Influences of Load on Coefficient of Friction (COF) of Monolithic TiB_2 and Doped TiB_2 with SiC

Figure 14 shows the tribological performance of the sintered materials. It revealed the average COF of the sintered composites. The average COF for the monolithic TiB_2 ceramic ranges from 0.16 to 0.47 with a rise in the load from 5 to 20 N. The average COF first increases and then decreases at load 5 N and 10 N, respectively, as depicted in Fig. 14, similarly the same trend was also observed for av. COF of this composite at 15 N and 20 N. The outcomes of monolithic TiB_2 demonstrated that lower average COF (0.16) could be achieved at a higher load of 20 N.

The average COF of TiB_2–10SiC varies in the range of 0.11–0.44 with an increase in the load. The average COF firstly increases and then decreases as the load increases. The lower average COF (0.11) was obtained at a lower and higher load of 10 N and 20 N, respectively. The average COF of TiB_2–20SiC varies in the range of 0.11–0.19 with an increase in the load. A recognizable and appreciable lower av. COF was attained for this composite (TiB_2–20SiC) at the loads 5 N–10 N in contrast to monolithic TiB_2 and TiB_2–10SiC composites.

The COF was observed to be high for the undoped TiB_2; however, it got reduced via the increment in the introduction of SiC (Fig. 14). The general decline in the COF for TiB_2–20SiC composite was attributed to the creation of a substantial amount of film by the additive (SiC), which lowered the COF of the ceramic composite [46]. Thus, this film minimizes the barrier to sliding movement between the contact point of the sample and the load.

3.6 The Influences of Load on Wear Rates of Monolithic TiB_2 and Doped TiB_2 with SiC

The wear rates of monolithic TiB_2 and reinforced composites with different percentages of SiC at different loads are depicted in Fig. 15. As the load increased from 5 to 20 N, the specific wear rates for the monolithic TiB_2 range from 9.403×10^{-5} to 5.149×10^{-4} mm^3/N.m. The specific wear rate of monolithic TiB_2 does not follow a linear pattern, as its specific wear rate first increases at 5 N load and then decreases at 10 N, but at 15 N and 20 N the specific wear rate increased again. Thus, the least wear rate was achieved at 10 N load, which signifies that at higher load, the undoped TiB_2 cannot withstand some higher range of load; this is similarly observed by Zhang et al. [47].

For the TiB_2–10SiC composites, the specific wear rates increased from 2.866×10^{-5} to 4.106×10^{-4} mm^3/N.m as the load increased from 5 to 20 N, while a similar trend was also observed for TiB_2-20SiC composites, but its wear rates range from 2.093×10^{-5} to 1.5524×10^{-5} mm^3/N.m. Therefore, the least wear rate of 2.866×10^{-5} and 2.093×10^{-5} was attained for TiB_2–10SiC and TiB_2–20SiC at 5 N load in contrast to monolithic TiB_2, which has a wear rate value of 3.498×10^{-4}, at a further load of 10 N, 15 N and 20 N, it was examined that the wear rates of the reinforced composites are less than the monolithic TiB_2.

The percentage increase in the sintering additive (SiC) influenced the wear rate reduction although got increased as the load increased. The wear rate of the monolithic TiB_2 was observed to be greater than the composites being reinforced with SiC, as depicted in Fig. 15. The composites with a greater percentage of SiC particles depicted the lesser wear

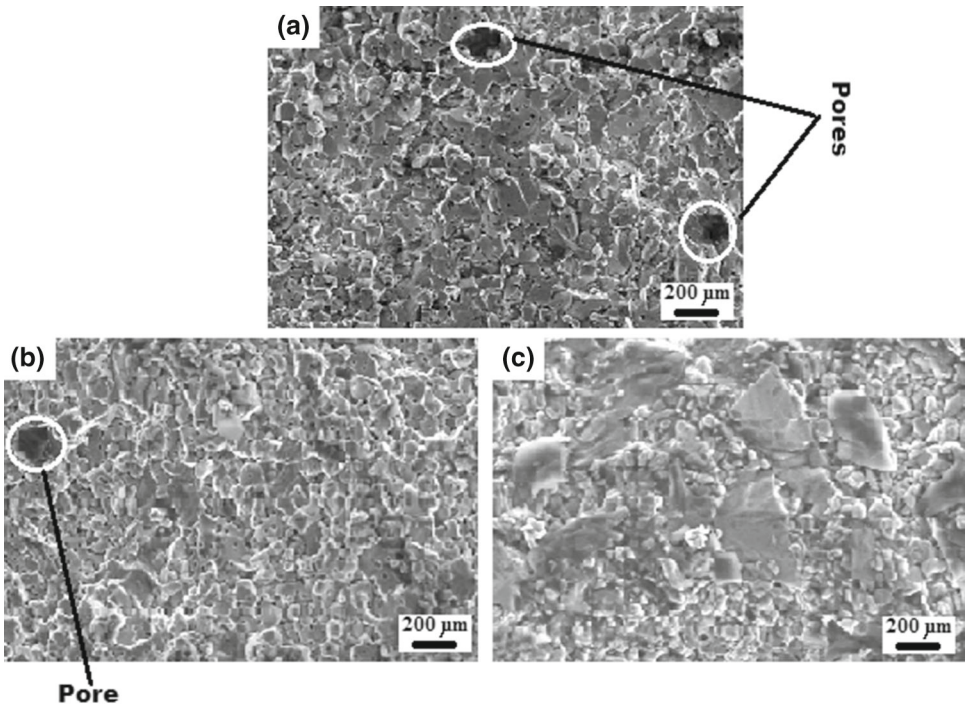

Fig. 11 SEM micrograph of fractured surfaces of **a** monolithic TiB_2, **b** TiB_2–10SiC and **c** TiB_2–20SiC sintered at 1850 °C for 10 min under 50 MPa: Showing the pores that are left after being sintered

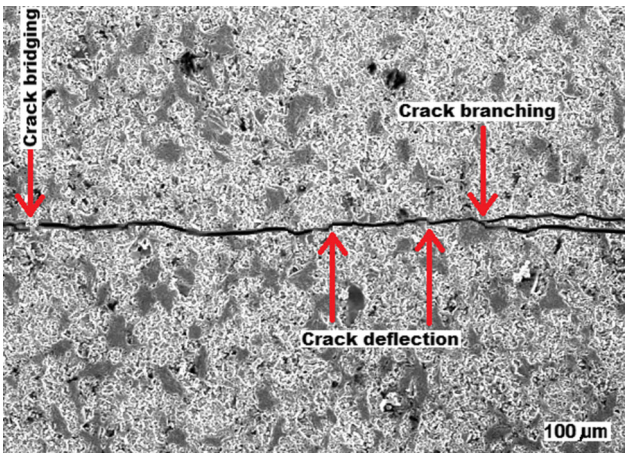

Fig. 12 SEM images of indentation crack depicting the toughening mechanisms for TiB_2–20SiC

rates, which were attributed to the solid interfacial bonding between the TiB_2 matrix and the SiC reinforcement. More also the optimum hardness and densification of TiB_2–20SiC assisted also in the attainment of good wear resistance. The enhancement in the wear resistance can also be credited to the efficient protection of SiC particles on the TiB_2 matrix, which limited the fracture and the plastic distortion of the composite [48]. It was further detected that TiB_2 and TiB_2/SiC (Figs. 16, 17 and 18) composites alter with microstructural variation during the sliding wear characteristics. High grains aspect ratio and hard interconnecting linkage of elongated grains initiated improved wear resistance. In addition, intergranular and secondary phases play a significant role in the friction and wear performance of TiB_2 matrix composites. Hence, the individual properties, compositions, etc. of these phases are a major contributor to the wear performance of the composites. Studies have shown that some phase developments in a composite have some depreciating effects in the wear performance while some phases could create some tribo-film in a sintered sample which when in contact with reciprocating load, there is wear reduction [49, 50].

3.7 Morphological Study of the Worn Surface

The worn-out surfaces of the synthesized composites regarding the applied load are presented in Figs. 16, 17 and 18. Scratches, debris and grooves were seen on the microstructure of the wear tracks. From the micrographs (Fig. 18), a small number of grooves in the form of scratches is depicted by the composite with a high percentage of SiC (TiB_2–20SiC), hence exhibiting excellent wear resistance. The microstructure of the composite with 10% SiC reinforcement shows some shallow grooves and slight delamination (Fig. 17). Large delamination on the microstructure of the monolithic TiB_2 (Fig. 16) was observed, when the load was increased from 15 to 20 N. The strong adhesion and bond between the sintering additive SiC and the ceramic matrix of TiB_2 could be liable for the creation of phases (TiC) that limit the wear of the sample's surface, hence improving the wear resistance. A similar observation by Raju et al. [51]

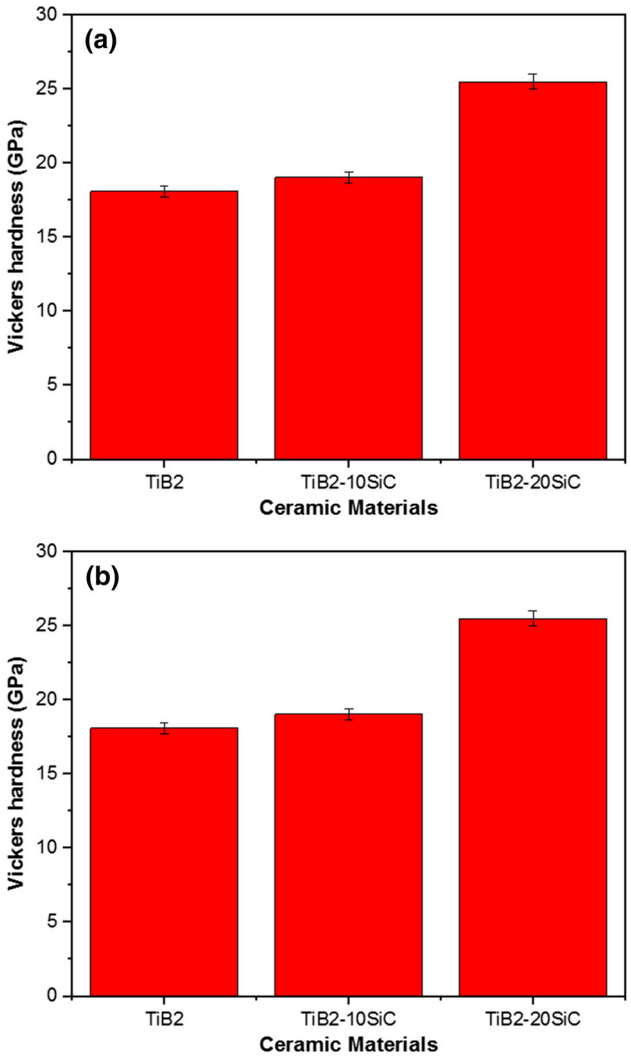

Fig. 13 Mechanical properties of monolithic TiB_2 and TiB_2 with SiC, **a** Vickers hardness, **b** Fracture toughness

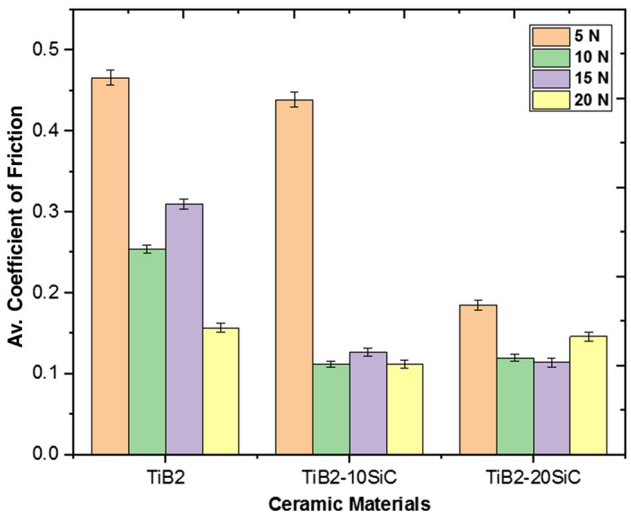

Fig. 14 Average COF of monolithic TiB_2 and doped TiB_2 with SiC

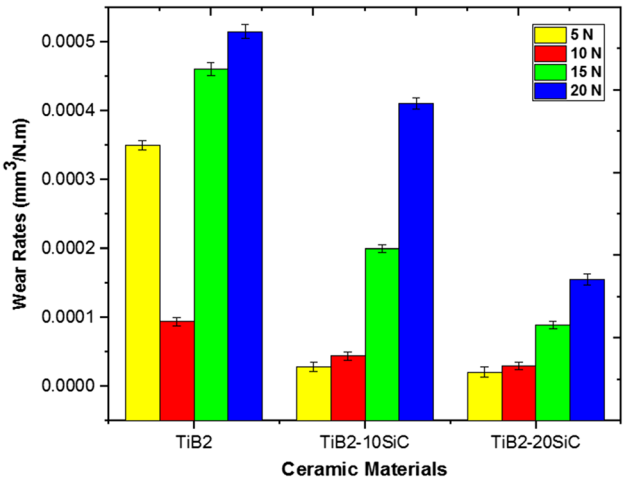

Fig. 15 Wear rates of monolithic TiB_2 and doped TiB_2 with SiC

established that the inclusion of particle additives in a matrix composite showed a morphology of minor scratches because there was strong bond created with the matrix alloy. Murthy et al. [29] discovered that the addition of ZrO_2 to B_4C ceramic matrix created in-situ ZrB_2 develops round pores of sub-micron size. Hence, the establishment of CO gas could aid to arrest or deflect cracks, thus enhancing the tribological behavior of B_4C ceramics.

4 The Effects of Microstructure, Densification and Mechanical Properties on the Wear Performance of TiB_2–SiC

The microstructure examination on TiB_2-SiC depicted that uniform distribution of the sintering additives was observed to influence the wear behavior of the composites. The discovered in-situ phase especially TiC formed had a high impact on the enhanced densification and consequently its mechanical properties (hardness, fracture toughness, etc.). Conversely, uneven distribution of these additives in the matrix and their mismatch between the matrix and the additives may lead to poor properties of the composites. Studies have been carried out that mechanical features such as fracture toughness, elastic modulus and hardness have had an immense impact on the wear performance of complicated brittle materials under sliding situations [30, 52, 53].

Concerning the effect of fracture toughness on the wear behavior of materials, the crack bridging and deflection caused by some amount of the sintering additives in the composites is a notable performance that contributes to the developed wear behavior of materials. More also, the resistibility of materials to a localized plastic deformation initiated via either mechanical abrasion or indenter, a term regarded as hardness, also impact on the tribology behavior

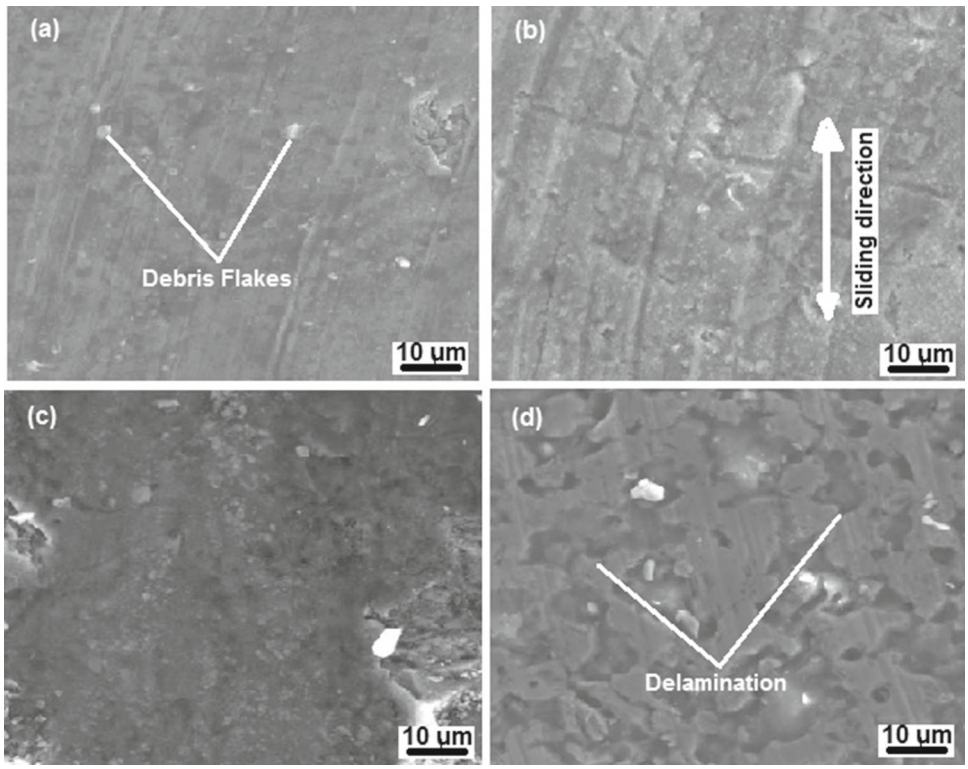

Fig. 16 SEM image of worn-out surfaces of monolithic TiB_2 at a load of **a** 5 N, **b** 10 N, **c** 15 N and **d** 20 N

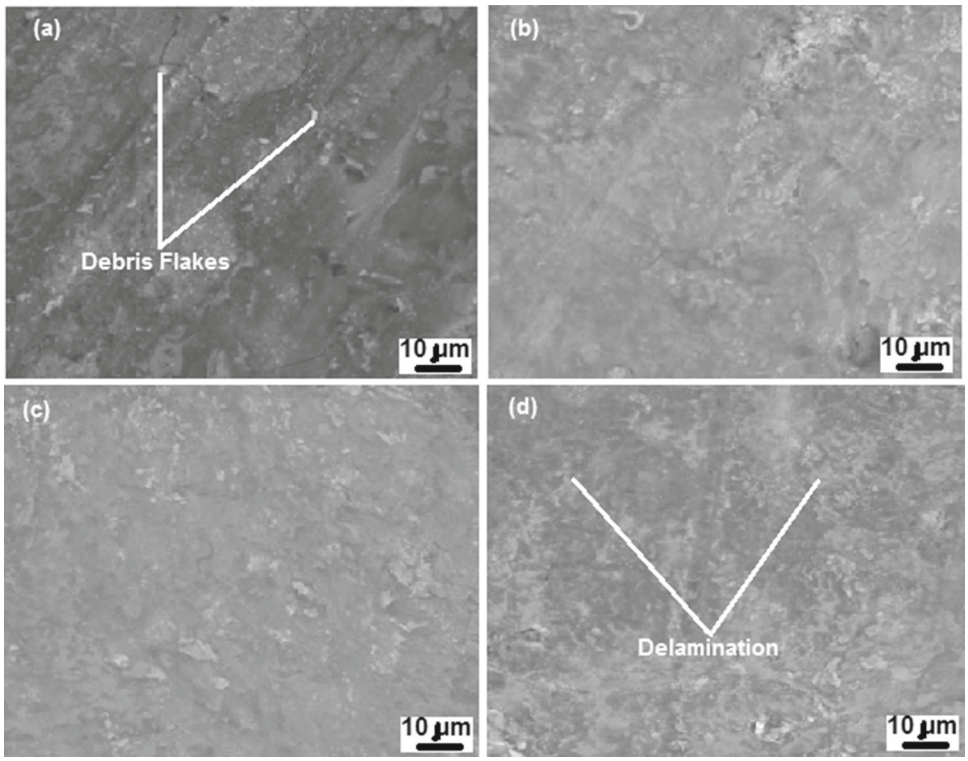

Fig. 17 SEM image of worn-out surfaces of TiB_2–10SiC at a load of **a** 5 N, **b** 10 N, **c** 15 N and **d** 20 N

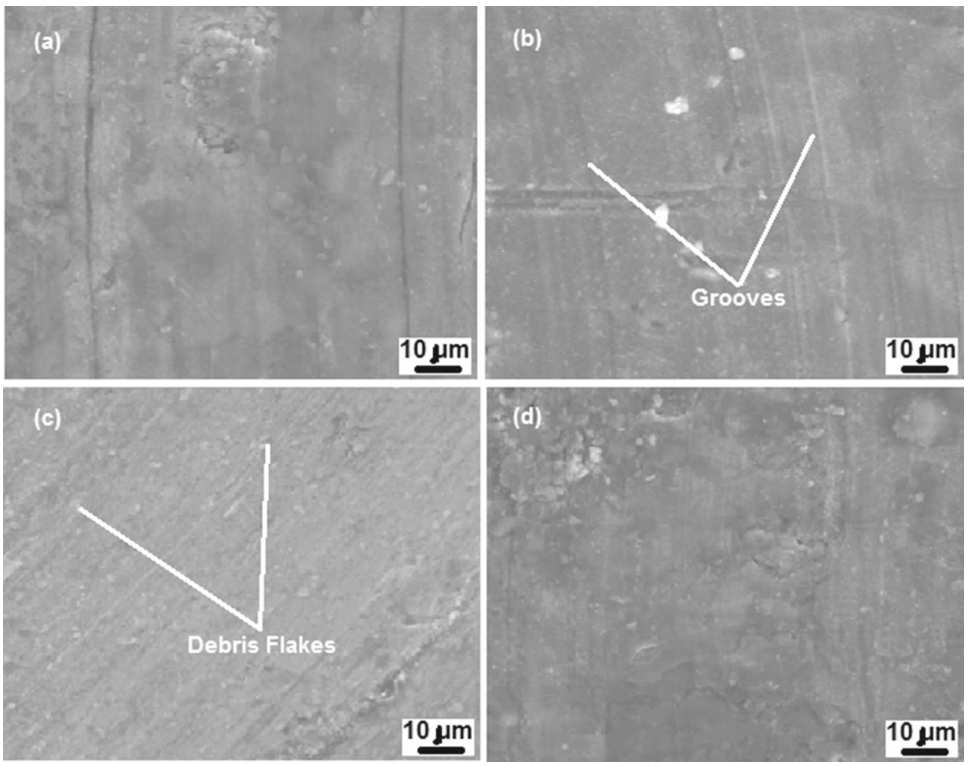

Fig. 18 SEM image of worn-out surfaces of TiB_2–20SiC at a load of **a** 5 N, **b** 10 N, **c** 15 N and **d** 20 N

of a material. Thus, the little removal of materials or scratches from the surface of sintered composites during the characterizing of their wear performance can be attributed to the hardness property of the material. The hardness or the solidity of materials is highly dependent on their strength, ductility, strain, elastic stiffness, toughness, plasticity, viscoelasticity. Consequently, the deficiency in some of these properties mentioned above in a material may lower its overall hardness property [54]. Significant research has been done to comprehend the impact of materials composition and experimental parameters under sliding conditions on the level of the material's deterioration. At the tribo-contact, some chemical layers are sometimes absent, and this initiates the sliding wear across the surface of the brittle components hence by the creation and spread of lateral cracks, the elimination of the materials occurs [30, 55, 56].

5 Conclusion

The synthesizing of monolithic TiB_2, as well as TiB_2–10%SiC and TiB_2–20%SiC composites, were achieved via SPS at 1850 °C for 10 min under 50 MPa. The following outcomes were discovered:

1. The densification increases as the percentage of the sintering additives increase from 0–20. The composite of TiB_2–20%SiC has the maximum theoretical density of 99.6%
2. One of the in-situ phases, especially TiC, was discovered to contribute to the enhancement in the mechanical properties
3. The wear performance is hugely linked to the composites, which have improved densification, hardness and fracture toughness. Thus the composites of TiB_2–20%SiC with relative density, hardness and fracture toughness of 99.5%, 25.5 GPa and 4.5 MPa.$m^{1/2}$, respectively, depicted the optimum wear resistance in contrast to other composites which has less or no addition of SiC (TiB_2, TiB_2-10%SiC). The creation of a substantial amount of film by the additive (SiC) minimized the barrier to sliding movement between the contact point of the sample and the load. Thus, the wear rates of the composites were reduced.

Authors Contributions All authors contributed to the study conception and design. Material preparation, data collection and analysis were performed by Mr. S. D OGUNTUYI, PROF. O. T JOHNSON AND Dr. M. B SHONGWE, Dr. L. TSHABALALA AND DR. N. MALATJI. The first draft of the manuscript was written by Mr. S. D OGUNTUYI and all authors commented on previous versions of the manuscript. All authors read and approved the final manuscript.

Funding This research was supported by the National Research Foundation of South Africa for the Grant, Unique Grant No. 117867.

Declarations

Conflict of interest Not Applicable.

References

1. Bilgi, E.; Camurlu, H.E.; Akgün, B.; Topkaya, Y.; Sevinç, N.: Formation of TiB_2 by volume combustion and mechanochemical process. Mater. Res. Bull. **43**, 873–881 (2008)
2. Shahbazi, M.; Tayebifard, S.A.; Razavi, M.: Effect of Ni content on the reaction behaviors and microstructure of TiB_2–TiC/Ni cermets synthesized by MASHS. Adv. Ceram. Prog. **2**, 22–26 (2016)
3. Zhang, Z.H.; Shen, X.B.; Wang, F.C.; Lee, S.K.; Wang, L.: Densification behavior and mechanical properties of the spark plasma sintered monolithic TiB_2 ceramics. Mater. Sci. Eng. A **527**, 5947–5951 (2010)
4. Mahaseni, Z.H.; Germi, M.D.; Ahmadi, Z.; Asl, M.S.: Microstructural investigation of spark plasma sintered TiB_2 ceramics with Si_3N_4 addition. Ceram. Int. **44**, 13367–13372 (2018)
5. Zheng, L.; Li, F.; Zhou, Y.: Preparation, microstructure, and mechanical properties of TiB_2 using $Ti_3 AlC_2$ as a sintering aid. J. Am. Ceram. Soc. **95**, 2028–2034 (2012)
6. Park, J.H.; Koh, Y.H.; Kim, H.E.; Hwang, C.S.; Kang, E.S.: Densification and mechanical properties of titanium diboride with silicon nitride as a sintering aid. J. Am. Ceram. Soc. **82**, 3037–3042 (1999)
7. Ahmadi, Z.; Nayebi, B.; Asl, M.S.; Farahbakhsh, I.; Balak, Z.: Densification improvement of spark plasma sintered TiB2-based composites with micron-, submicron-and nano-sized SiC particulates. Ceram. Int. **44**, 11431–11437 (2018)
8. Ogunbiyi, O.F.; Jamiru, T.; Sadiku, E.R.; Beneke, L.W.; Adesina, O.T.; Adegbola, T.A.: Microstructural characteristics and thermophysical properties of spark plasma sintered Inconel 738LC. Int. J. Adv. Manuf. Technol. **104**, 1425–1436 (2019)
9. Bhaumik, S.K.; Divakar, C.; Singh, A.K.; Upadhyaya, G.S.: Synthesis and sintering of TiB_2 and TiB_2–TiC composite under high pressure. Mater. Sci. Eng. A **279**, 275–281 (2000)
10. Shongwe, M.B.: Spark plasma sintering of ceramic matrix composite of TiC: microstructure, densification, and mechanical properties: a review. In: Advances in Material Science and Engineering: Selected Articles from ICMMPE 2020, p. 93 (2020)
11. Farhadi, K.; Namini, A.S.; Asl, M.S.; Mohammadzadeh, A.; Kakroudi, M.G.: Characterization of hot pressed SiC whisker reinforced TiB_2 based composites. Int. J. Refract Metal Hard Mater. **61**, 84–90 (2016)
12. Asl, M.S.; Ahmadi, Z.; Parvizi, S.; Balak, Z.; Farahbakhsh, I.: Contribution of SiC particle size and spark plasma sintering conditions on grain growth and hardness of TiB_2 composites. Ceram. Int. **43**, 13924–13931 (2017)
13. Muraoka, Y.; Yoshinaka, M.; Hirota, K.; Yamaguchi, O.: Hot isostatic pressing of TiB_2–ZrO_2 (2 mol% Y_2O_3) composite powders. Mater. Res. Bull. **31**, 787–792 (1996)
14. Oguntuyi, S.D.; Johnson, O.T.; Shongwe, M.B.: Spark plasma sintering of ceramic matrix composite of TiC: microstructure, densification, and mechanical properties: a review. Int. J. Adv. Manuf. Technol. **116**, 69–82 (2021)
15. Jiang, D.; Van der Biest, O.; Vleugels, J.: ZrO_2–WC nanocomposites with superior properties. J. Eur. Ceram. Soc. **27**, 1247–1251 (2007)
16. Oguntuyi, S.D.; Johnson, O.T.; Shongwe, M.B.: Spark plasma sintering of ceramic matrix composite of ZrB_2 and TiB_2: microstructure, densification, and mechanical properties—a review. In: Metals and Materials International, pp. 1–14 (2020)
17. Balak, Z.; Zakeri, M.; Rahimipoor, M.R.; Salahi, E.; Azizieh, M.; Kafashan, H.: Investigation of effective parameters on densification of ZrB_2-SiC based composites using taguchi method. Adv. Ceram. Prog. **2**, 7–15 (2016)
18. Balak, Z.; Azizieh, M.: Oxidation of ZrB_2-SiC composites at 1600 C: effect of carbides, borides, silicides, and chopped carbon fiber. Adv. Ceram. Prog. **4**, 18–23 (2018)
19. Oguntuyi, S.D.; Johnson, O.T.; Shongwe, M.B.; Jeje, S.O.; Rominiyi, A.L.: The effects of sintering additives on the ceramic matrix composite of ZrO_2: microstructure, densification, and mechanical properties—a review. In: Advances in Applied Ceramics, pp. 1–17 (2021)
20. Zhang, W.; Yamashita, S.; Kita, H.: Progress in tribological research of SiC ceramics in unlubricated sliding—a review. Mater. Des. **190**, 108528 (2020)
21. Ogunbiyi, O.F.; Sadiku, E.R.; Jamiru, T.; Adesina, O.T.; Beneke, L.W.: Spark plasma sintering of Inconel 738LC: densification and microstructural characteristics. Mater. Res. Express **6**, 1065g8 (2019)
22. Namini, A.S.; Gogani, S.N.S.; Asl, M.S.; Farhadi, K.; Kakroudi, M.G.; Mohammadzadeh, A.: Microstructural development and mechanical properties of hot pressed SiC reinforced TiB_2 based composite. Int. J. Refract. Metal Hard Mater. **51**, 169–179 (2015)
23. Asl, M.S.; Namini, A.S.; Kakroudi, M.G.: Influence of silicon carbide addition on the microstructural development of hot pressed zirconium and titanium diborides. Ceram. Int. **42**, 5375–5381 (2016)
24. Asl, M.S.; Delbari, S.A.; Shayesteh, F.; Ahmadi, Z.; Motallebzadeh, A.: Reactive spark plasma sintering of TiB_2–SiC–TiN novel composite. Int. J. Refract. Metal Hard Mater. **81**, 119–126 (2019)
25. Ahmadi, Z.; Hamidzadeh Mahaseni, Z.; Dashti Germi, M.; Shahedi Asl, M.: Microstructure of spark plasma sintered TiB_2 and TiB_2–AlN ceramics. Adv. Ceram. Prog. **5**, 36–40 (2019)
26. Kim, H.J.; Choi, H.J.; Lee, J.G.: Mechanochemical synthesis and pressureless sintering of TiB_2–AlN composites. J. Am. Ceram. Soc. **85**, 1022–1024 (2002)
27. Shayesteh, F.; Delbari, S.A.; Ahmadi, Z.; Shokouhimehr, M.; Asl, M.S.: Influence of TiN dopant on microstructure of TiB_2 ceramic sintered by spark plasma. Ceram. Int. **45**, 5306–5311 (2019)
28. Alexander, R.; Ravikanth, K.V.; Bedse, R.D.; Murthy, T.S.R.C.; Dasgupta, K.: Effect of carbon fiber on the tribo-mechanical properties of boron carbide: comparison with carbon nanotube reinforcement. Int. J. Refract. Metal Hard Mater. **85**, 105055 (2019)
29. Murthy, T.; Ankata, S.; Sonber, J.K.; Sairam, K.; Singh, K.; Nagaraj, A., et al.: Microstructure, thermo-physical, mechanical and wear properties of in-situ formed boron carbide-zirconium diboride composite. Ceram. Silik. **62**, 15–30 (2018)
30. Sharma, S.K.; Kumar, B.V.M.; Kim, Y.-W.: Effect of WC addition on sliding wear behavior of SiC ceramics. Ceram. Int. **41**, 3427–3437 (2015)
31. Sonber, J.K.; Limaye, P.K.; Murthy, T.S.R.C.; Sairam, K.; Nagaraj, A.; Soni, N.L., et al.: Tribological properties of boron carbide in sliding against WC ball. Int. J. Refract. Metal Hard Mater. **51**, 110–117 (2015)
32. Fukuhara, M.; Fukazawa, K.; Fukawa, A.: Physical properties and cutting performance of silicon nitride ceramic. Wear **102**, 195–210 (1985)
33. Anstis, G.R.; Chantikul, P.; Lawn, B.R.; Marshall, D.B.: A critical evaluation of indentation techniques for measuring fracture toughness: I, direct crack measurements. J. Am. Ceram. Soc. **64**, 533–538 (1981)
34. Evans, A.G.; Charles, E.A.: Fracture toughness determinations by indentation. J. Am. Ceram. Soc. **59**, 371–372 (1976)
35. Asl, M.S.: Microstructure, hardness and fracture toughness of spark plasma sintered ZrB_2–SiC–Cf composites. Ceram. Int. **43**, 15047–15052 (2017)

36. Farahbakhsh, I.; Ahmadi, Z.; Asl, M.S.: Densification, microstructure and mechanical properties of hot pressed ZrB_2–SiC ceramic doped with nano-sized carbon black. Ceram. Int. **43**, 8411–8417 (2017)
37. Asl, M.S.; Farahbakhsh, I.; Nayebi, B.: Characteristics of multi-walled carbon nanotube toughened ZrB_2–SiC ceramic composite prepared by hot pressing. Ceram. Int. **42**, 1950–1958 (2016)
38. Nguyen, V.-H.; Delbari, S.A.; Namini, A.S.; Ahmadi, Z.; Van Le, Q.; Shokouhimehr, M., et al.: Microstructural evolution of TiB_2–SiC composites empowered with Si_3N_4, BN or TiN: a comparative study. Ceram. Int. **47**, 1002–1011 (2021)
39. Ghafuri, F.; Ahmadian, M.; Emadi, R.; Zakeri, M.: Effects of SPS parameters on the densification and mechanical properties of TiB_2-SiC composite. Ceram. Int. **45**, 10550–10557 (2019)
40. Asl, M.S.; Kakroudi, M.G.; Rezvani, M.; Golestani-Fard, F.: Significance of hot pressing parameters on the microstructure and densification behavior of zirconium diboride. Int. J. Refract. Metal Hard Mater. **50**, 140–145 (2015)
41. King, D.S.; Fahrenholtz, W.G.; Hilmas, G.E.: Microstructural effects on the mechanical properties of SiC-15 vol% TiB_2 particulate-reinforced ceramic composites. J. Am. Ceram. Soc. **96**, 577–583 (2013)
42. Lin, J.; Yang, Y.; Zhang, H.; Gong, J.: Effects of CNTs content on the microstructure and mechanical properties of spark plasma sintered TiB_2-SiC ceramics. Ceram. Int. **43**, 1284–1289 (2017)
43. Chen, H.; Wang, Z.; Wu, Z.: Investigation and characterization of densification, processing and mechanical properties of TiB_2–SiC ceramics. Mater. Des. **64**, 9–14 (2014)
44. Momeni, M.M.; Mirhosseini, M.; Chavoshi, M.: Growth and characterization of Ta_2O_5 nanorod and WTa_2O_5 nanowire films on the tantalum substrates by a facile one-step hydrothermal method. Ceram. Int. **42**, 9133–9138 (2016)
45. Demirskyi, D.; Sakka, Y.; Vasylkiv, O.: High-temperature reactive spark plasma consolidation of TiB_2–NbC ceramic composites. Ceram. Int. **41**, 10828–10834 (2015)
46. Aizawa, T.; Akhadejdamrong, T.; Mitsuo, A.: Self-lubrication of nitride ceramic coating by the chlorine ion implantation. Surf. Coat. Technol. **177**, 573–581 (2004)
47. Zhang, W.; Yamashita, S.; Kita, H.: Effects of load on tribological properties of B4C and B4C-SiC ceramics sliding against SiC balls. J. Asian Ceram. Soc. **8**, 586–596 (2020)
48. Kaviti, R.V.P.; Jeyasimman, D.; Parande, G.; Gupta, M.; Narayanasamy, R.: Investigation on dry sliding wear behavior of Mg/BN nanocomposites. J. Magn. Alloys **6**, 263–276 (2018)
49. Ogunbiyi, O.; Jamiru, T.; Sadiku, R.; Adesina, O.; Adesina, O.S.; Olorundaisi, E.: Influence of Nickel powder particle size on the microstructure and densification of spark plasma sintered Nickel-based superalloy. Int. J. Eng. Res. Afr. **53**, 1–19 (2021)
50. Ogunbiyi, O.; Jamiru, T.; Sadiku, R.; Beneke, L.; Adesina, O.; Fayomi, J.: Influence of sintering temperature on the corrosion and wear behaviour of spark plasma–sintered Inconel 738LC alloy. Int. J. Adv. Manuf. Technol. **104**, 4195–4206 (2019)
51. Raju, P.V.K.; Rajesh, S.; Rao, J.B.; Bhargava, N.: Tribological behavior of Al–Cu alloys and innovative Al–Cu metal matrix composite fabricated using stir-casting technique. Mater. Today Proc. **5**, 885–896 (2018)
52. Kumar, B.V.M.; Kim, Y.-W.; Lim, D.-S.; Seo, W.-S.: Influence of small amount of sintering additives on unlubricated sliding wear properties of SiC ceramics. Ceram. Int. **37**, 3599–3608 (2011)
53. Basu, B.; Kalin, M.: Tribology of Ceramics and Composites: A Materials Science Perspective. Wiley, New York (2011)
54. LaSalvia, J.C.; Campbell, J.; Swab, J.J.; McCauley, J.W.: Beyond hardness: ceramics and ceramic-based composites for protection. Jom **62**, 16–23 (2010)
55. Evans, A.G.: Wear mechanisms in ceramics. In: Fundamentals Friction and Wear of Materials (1981)
56. Tewari, A.; Basu, B.; Bordia, R.K.: Model for fretting wear of brittle ceramics. Acta Mater. **57**, 2080–2087 (2009)